ISSN 1070-3284, Russian Journal of Coordination Chemistry, 2023, Vol. 49, No. 9, pp. 577–592. © Pleiades Publishing, Ltd., 2023.
Russian Text © The Author(s), 2023, published in Koordinatsionnaya Khimiya, 2023, Vol. 49, No. 9, pp. 565–581.

Triphenylphosphine Thiolate Gold(I) Complexes with Redox-Active Schiff Bases: Synthesis, Electrochemical Properties, and Biological Activity

I. V. Smolyaninov[a], *, D. A. Burmistrova[a], N. P. Pomortseva[a], M. A. Polovinkina[b], O. P. Demidov[c], N. R. Al'myasheva[d], A. I. Poddel'skii[e], and N. T. Berberova[a]

[a] *Astrakhan State Technical University, Astrakhan, Russia*

[b] *Federal Research Center, Southern Scientific Center, Russian Academy of Sciences, Rostov-on-Don, Russia*

[c] *North Caucasus Federal University, Stavropol, Russia*

[d] *Gause Institute of New Antibiotics, Moscow, Russia*

[e] *Razuvaev Institute of Organometallic Chemistry, Russian Academy of Sciences, Nizhny Novgorod, Russia*

**e-mail: ivsmolyaninov@gmail.com*

Received February 13, 2023; revised March 15, 2023; accepted March 16, 2023

Abstract—New gold(I) phosphine thiolate complexes [$(Ph_3P)Au(SL^n)$] **I**–**V** with Schiff bases L^nSH containing redox-active catechol, phenol, or quinone methide moieties were synthesized and characterized. The molecular structure of compound **I** in the crystalline state was established by X-ray diffraction (CCDC no. 2237815). The electrochemical behavior of compounds **I**–**V** was studieв by cyclic voltammetry. The proposed electrooxidation mechanism of the complexes involves the Au–S bond cleavage, the disulfide formation, as well as the oxidation of the redox active group of the ligand. In the cathode region, complexes **I**–**III** tend to form relatively stable monoanionic species. The radical scavenging activity of complexes decreases in comparison to free ligands in the reactions with synthetic radicals and the CUPRAC test. Compounds **I**, **II**, **IV**, and **V** have no clear-cut effect on the promoted DNA damage; however, they show antioxidant action in the non-enzymatic lipid peroxidation of rat liver homogenate. Compounds **I**–**V** demonstrate a weak antibacterial activity against *Staphylococcus aureus* strains. The gold(I) complexes cytotoxicity was studied against A-549, MCF-7, and HTC-116 cancer cell lines using MTT assay. The test compounds are characterized by higher selectivity to certain types of cells than the sulfur-containing Schiff bases. The presence of quinone methide moiety in the ligand in case of **V** significantly increases the cytotoxicity against all of the cell lines.

Keywords: gold(I) thiolate complexes, redox active Schiff bases, X-ray diffraction, cyclic voltammetry, antioxidant activity, cytotoxicity

DOI: 10.1134/S1070328423600420

INTRODUCTION

Gold(I/III) coordination compounds have attracted the attention of researchers because of their catalytic properties, luminescence, diverse biological activities, and wide potential applications in materials chemistry [1]. In addition to platinum(II) compounds used in the cancer therapy and antimony(III/V) derivatives employed as antiparasitic agents, a number of gold(I) compounds are metal-containing pharmaceutical drugs approved for the treatment of rheumatoid arthritis. Structurally, these compounds (auranofin, aurothioglucose, and aurothiomalate) are gold(I) thiolate complexes; they possess anti-inflammatory and antitumor activities [2, 3]. In particular, it was found that auranofin and other gold(I) compounds with biologically active ligands have an inhibitory effect on thioredoxin reductase (TrxR) [4].

Thioredoxin reductase is a key biological target for gold(I) compounds, because its inhibition is accompanied by generation of reactive oxygen species (superoxide radical anion and hydrogen peroxide), which leads to a change in the redox state of cells, disruption of the integrity of biomacromolecules (proteins, lipids, and DNA) and tissue damage. This produces oxidation stress and gives rise to cytotoxicity. However, this effect occurs not only in malignant cells, but also in healthy cells. The development of new metal-containing therapeutic agents is hampered by toxicity and low selectivity of these compounds. One of solutions to this problem is to use ligand prooxidant containing antioxidant groups (sterically hindered phenol, synthetic vitamin E analogues, cysteine, acetylcysteine, and glutathione). A rational design of this type of complexes can be useful for modulating the

cytotoxicity and anti/pro-oxidant activity and generally lead to mitigation of side effects [5–7].

Schiff bases, which are widely used as ligands in coordination chemistry, considerably influence the bioactivity of complex compounds. Relatively well-studied systems are Au(III) complexes with Schiff bases, acting as potential antitumor agents, which is due to their structural features, high thermodynamic stability, and lipophilicity [8, 9]. The Au(I) alkynyl complexes with Schiff bases containing phenol groups showed anticancer activity in vitro comparable with the cisplatin activity [10]. Meanwhile, there are few gold(I) thiolate complexes with Schiff bases [11]. Previously, we have synthesized Schiff bases containing a thiol group and redox active fragments. This combination allows to influence the electrochemical properties and biological activity [12]. The coordination of the thiol group to the gold(I) atom and formation of the corresponding thiolate complexes may considerably affect the properties of compounds.

The purpose of this study is to obtain new gold(I) thiolate complexes containing ligands with azomethine linker and a phenol or catechol moiety, to investigate the electrochemical properties and anti/pro-oxidant activity of these complexes, and to assess their in vitro cytotoxicity against several cancer cell lines.

EXPERIMENTAL

The following commercial reagents were used as received: [(Ph_3P)AuCl] (Aldrich, 99%), *n*-tetrabutylammonium perchlorate (*n*-Bu_4NClO_4) (Alfa Aesar, 99%), 2,2'-azo-bis(2-amidinopropane) dihydrochloride (AAPH, Aldrich, 97%), 2,2'-azino-bis(3-ethylbenzothiazoline-6-sulfonic acid) (ABTS, ≥98%, TCI), 2,2'-diphenyl-1-picrylhydrazyl (DPPH) radical (Aldrich), thiobarbituric acid (≥98%, Sigma-Aldrich), deoxyribonucleic acid (DNA) sodium salt from salmon testes (Sigma), phosphate buffer pH 7.4 (Sigma), 6-hydroxy-2,5,7,8-tetramethylchromane-2-carboxylic acid (Trolox, 97%, Aldrich), trichloroacetic acid (≥99%, Sigma-Aldrich), 2,9-dimethyl-1,10-phenanthroline (neocuproine) (99%, Aldrich), copper(II) chloride (97%, Sigma-Aldrich), ethylenediaminotetraacetic acid (≥99%, Sigma-Aldrich), 3,7-dihydropurine-2,6-dione (xanthine, ≥99%, Sigma-Aldrich), bovine serum albumin (≥96%, Sigma-Aldrich), xanthine oxidase (Sigma-Aldrich, grade IV), tetrazolium blue (90%, Alfa Aesar), Dulbecco's modified eagle's medium (DMEM medium, PanEco, Russia), Mueller Hinton broth (MHB, PanEco, Russia), L-glutamine (PanEco, Russia), fetal calf serum (Hyclone, Austria), ciprofloxacin (AppliChem Biochemica Chemical Synthesis Services, for biochemistry), penicillin (PanEco, Russia), streptomycin (PanEco, Russia), and 3-(4,5-dimethylthiazol-2-yl)-2,5-diphenyltetrazolium bromide (MTT, PanEco, Russia). Schiff bases (L^nSH) were prepared by a previously described procedure [12]. The solvents used in the study were purified and dehydrated by standard procedures [13].

^1H and ^{13}C NMR spectra were recorded on a Bruker AVANCE HD 400 spectrometer operating at 400 MHz (^1H) and 100 MHz (^{13}C) using tetramethylsilane as the internal standard and $CDCl_3$ as the solvent. IR spectra were measured on an FSM 1201 spectrometer in KBr pellets. Elemental analysis was carried out on a Euro EA 3000 analyzer (C,H,N). Electronic absorption spectra were recorded on an SF-104 spectrophometer (300–600 nm range) at room temperature. The electrochemical potentials of the compounds in acetonitrile were measured by cyclic voltammetry (CV) in a three-electrode cell under argon using an IPC-pro potentiostat. A stationary glassy carbon (GC) working electrode (2 mm in diameter) and a platinum plate ($S = 18$ mm^2) auxiliary electrode were used. A reference electrode (Ag/AgCl/KCl) with a water-proof diaphragm was used. The concentration of compounds was 0.003 mol/L. The number of electrons transferred in the electrode process was estimated relative to the ferrocene standard. The potential sweep rate was 0.2 V s^{-1}. The supporting electrolyte was 0.1 M *n*-Bu_4NClO_4.

Synthesis of gold(I) compounds [(Ph_3P)Au(SL^n)] (I–V). One equivalent of Schiff base L^nSH (0.2 mmol) in acetonitrile (2 mL) was added to a solution of [(Ph_3P)AuCl] (0.2 mmol) in acetonitrile (3 mL), the solution was deaerated by purging with argon (5 min), and one equiv. of triethylamine was added. The reaction of the ligand with [(Ph_3P)AuCl] was accompanied by color change to orange-red for catechol-containing Schiff bases or to bright yellow for compounds containing a sterically hindered phenol moiety. The solution was left for 3 days at room temperature. The precipitate was collected on a filter, washed with hexane, and dried in vacuo.

[(Ph_3P)Au(SL^1)] (I). The yield of **I** as dark cherry-colored crystals was 0.140 g (86%). IR (KBr; ν, cm^{-1}): 3371, 3051, 2954, 2906, 2870, 1601, 1558, 1540, 1506, 1480, 1465, 1437, 1418, 1395,1381,1363, 1297, 1258, 1220, 1190, 1162, 1100.

^1H NMR (400 MHz; $CDCl_3$, δ, ppm): 1.43 and 1.49 (both s, 9H each, 2*t*-Bu), 6.49 (s, 1H, OH), 6.75 (s, 1H, C_6H_1), 7.08 (d, $^3J(H,H) = 8.5$ Hz, 2H, arom. C_6H_4), 7.43–7.61 (m, 16H, 15H, arom. C_6H_5, +1H, OH), 7.66 (d, $^3J(H,H) = 8.5$ Hz, 2H, arom. C_6H_4), 9.30 (s, 1H, CH=N).

^{13}C NMR (100 MHz; $CDCl_3$; δ, ppm): 29.16, 33.27, 35.16, 35.58, 112.40, 113.36, 120.28, 129.04, 129.18, 129.29, 129.61, 131.74, 131.77, 133.49, 134.09,

134.23, 136.36, 140.03, 141.44, 141.71, 142.54, 156.08, 158.82.

For $C_{39}H_{41}NO_2SPAu$

Anal. calcd., %	C, 57.42	H, 5.07	N, 1.72
Found, %	C, 57.50	H, 5.21	N, 1.69

[(Ph_3P)Au(SL^2)] (II). The yield of **II** as a brick red powder was 0.080 g (49%). IR (KBr; ν, cm^{-1}): 3503, 3478, 3060, 2954, 2909, 2867, 1604, 1576, 1552, 1480, 1465, 1435, 1400, 1387, 1364, 1244, 1222, 1162, 1131, 1100. ^{1}H NMR (400 MHz; $CDCl_3$; δ, ppm): 1.40 and 1.46 (both s, 9H each, 2^{t}Bu), 6.65 (s, 1H, arom. C_6H_1), 6.83 (br.s, 1H, OH), 7.04 (td, ^3J(H,H) = 7.4 Hz, ^4J(H,H) = 1.6 Hz, 1H, arom. C_6H_4), 7.12 (td, ^3J(H,H) = 7.4 Hz, ^4J(H,H) = 1.6 Hz, 1H, arom. C_6H_4), 7.16 (dd, ^3J(H,H) = 7.6 Hz, ^4J(H,H) = 1.6 Hz, 1H, arom. C_6H_4), 7.35–7.52 (m, 15H, arom. C_6H_5), 7.90 (d, ^3J(H,H) = 7.6 Hz, 1H, arom. C_6H_4), 9.26 (d, J(H,H) = 5.6 Hz, 1H, CH=N). ^{13}C NMR ($CDCl_3$, 100 MHz, δ, ppm): 29.17, 33.30, 35.05, 35.54, 111.73, 112.71, 117.42, 125.83, 129.08, 129.19, 129.64, 131.58, 131.60, 134.09, 134.23, 136.06, 139.61, 143.53, 144.97, 157.33, 161.21.

For $C_{39}H_{41}NO_2SPAu$

Anal. calcd., %	C, 57.42	H, 5.07	N, 1.72
Found, %	C, 57.48	H, 5.26	N, 1.75

[(Ph_3P)Au(SL^3)] (III). The yield of **III** as a bright red powder was 0.081 g (46%). IR (KBr; ν, cm^{-1}): 3507, 3302, 3054, 2962, 2909, 2874, 1597, 1588, 1547, 1479, 1436, 1403, 1383, 1323, 1256, 1218, 1162, 1128, 1101. ^{1}H NMR (400 MHz; $CDCl_3$; δ, ppm): 1.42 (s, 9H, ^{t}Bu), 1.48 (s, 9H, ^{t}Bu), 6.46 (s, 1H, OH), 6.76 (s, 1H, arom. C_6H_1), 7.25 (d, ^3J(H,H) = 7.9 Hz, 1H, arom. C_6H_3), 7.27 (s, 1H, arom. C_6H_3), 7.40–7.55 (m, 15H, Ph), 8.01 (d, ^3J(H,H) = 7.9 Hz, 1H, arom. C_6H_3), 9.32 (d, ^3J(H,H) = 2.3 Hz, 1H, CH=N), 15.90 (d, ^3J(H,H) = 2.3 Hz, 1H, NH^+). ^{13}C NMR (100 MHz; $CDCl_3$; δ, ppm): 29.14, 33.35, 35.19, 35.60, 112.71, 113.61, 114.56 (q, ^2J(C,F) = 4.0 Hz), 121.85, 126.92 (q, ^1J(C,F) = 32.3 Hz), 128.84, 129.22 (d, ^4J(C,P) = 11.4 Hz), 129.41, 131.75 (d, ^5J(C,P) = 2.3 Hz), 134.12 (d, ^3J(C,P) = 13.6 Hz), 135.57, 136.58, 140.34, 142.47, 142.76, 146.94, 156.51, 160.21.

For $C_{40}H_{40}NO_2F_3SPAu$

Anal. calcd., %	C, 54.36	H, 4.56	N, 1.58
Found, %	C, 54.43	H, 4.67	N, 1.56

[(Ph_3P)Au(SL^4)] (IV). The yield of **IV** as a yellow finely crystalline powder was 0.120 g (75%). IR (KBr; ν, cm^{-1}): 3057, 2957, 2907, 2864, 1594, 1574, 1552, 1480, 1463, 1437, 1393, 1358, 1269, 1250, 1196, 1170, 1104. ^{1}H NMR (400 MHz; $CDCl_3$; δ, ppm): 1.33 and 1.47 (both s, 9H each, 2^{t}Bu), 7.10 (d, 2H, ^3J(H,H) = 8.5 Hz, arom. C_6H_4), 7.19 (d, ^4J(H,H) = 2.2 Hz, 1H, arom. C_6H_2), 7.42 (d, ^4J(H,H) = 2.2 Hz, 1H, arom. C_6H_2), 7.45–7.60 (m, 15 H, arom. C_6H_5), 7.63 (d, ^3J(H,H) = 8.4 Hz, 2 H, arom. C_6H_4), 8.62 (s, 1H, CH=N), 13.94 (s, 1H, OH). ^{13}C NMR (100 MHz; $CDCl_3$; δ, ppm): 29.40, 31.46, 34.14, 35.03, 118.44, 120.87, 126.48, 127.42, 129.09, 129.17, 129.28, 129.65, 131.71, 131.74, 133.23, 134.11, 134.25, 136.73, 140.31, 140.63, 144.30, 158.11, 161.41.

For $C_{39}H_4NOSPAu$

Anal. calcd., %	C, 58.57	H, 5.17	N, 1.75
Found, %	C, 58.64	H, 5.31	N, 1.72

[(Ph_3P)Au(SL^5)] (V). The yield of **V** as a bright yellow finely crystalline powder was 0.105 g (66%). IR (KBr; ν, cm^{-1}): 3287, 3054, 2997, 2951, 2915, 2861, 1620, 1576, 1558, 1507, 1480, 1448, 1436, 1384, 1360, 1302, 1280, 1202, 1160, 1101. ^{1}H NMR (400 MHz; $CDCl_3$; δ, ppm): 1.18 and 1.38 (both s, 9H each, ^{t}Bu), 6.92 (m, 1H, arom. C_6H_4), 7.05 (d, ^4J(H,H) = 2.4 Hz, 1H, arom. C_6H_2), 7.10–7.17 (m, 1H, arom. C_6H_4), 7.15 (s, 1 H, OH), 7.32–7.52 (m, 15 H, arom. C_6H_5, +1H, arom. C_6H_4), 7.60 (d, ^4J(H,H) = 2.4 Hz, 1H, arom. C_6H_2), 7.72 (d, ^3J(H,H) = 7.6 Hz, 1H, arom. C_6H_4), 9.57 (d, ^4J(H,H) = 14.4 Hz, 1H, CH=N). ^{13}C NMR (100 MHz, $CDCl_3$, δ, ppm): 29.37, 29.49, 34.82, 35.16, 109.75, 111.80, 122.17, 122.67, 126.35, 128.20, 129.16, 129.28, 131.78, 133.11, 134.02, 134.16, 136.22, 138.88, 139.09, 143.26, 146.09, 184.61.

For $C_{39}H_4NOSPAu$

Anal. calcd., %	C, 58.57	H, 5.17	N, 1.75
Found, %	C, 58.52	H, 5.28	N, 1.71

X-ray diffraction. The crystals of **I** suitable for X-ray diffraction were obtained by slow evaporation of acetonitrile at room temperature. The set of experimental data was collected on an Agilent SuperNova diffractometer using a microfocus X-ray source with a copper anode and an Atlas S2 CCD array detector. The collection of reflections and determination and refinement of unit cell parameters were carried out using a dedicated CrysAlisPro 1.171.38.41 program package [14]. The structures were solved using the ShelXT software [15] and refined with the ShelXL software [16]. The hydrogen atom positions were found from the Fourier electron density maps and refined in the isotropic riding model. The crystallographic data and structure refinement details for **I** are summarized in Table 1.

Table 1. Crystallographic data and X-ray experiment details for complex **I**

Parameter	Value
Molecular formula	$C_{39}H_{41}AuNO_2PS$
M	815.72
T, K	293
Crystal system	Triclinic
Space group	$P\bar{1}$
a, Å	8.93560(10)
b, Å	14.6351(2)
c, Å	15.3504(2)
α, deg	106.9570(10)
β, deg	104.1710(10)
γ, deg	101.2430(10)
V, Å^3	1783.27(4)
Z	2
ρ(calcd.), mg/m^3	1.519
μ, mm^{-1}	4.262
θ, deg	$6.32 \le 2\theta \le 68.674$
Number of measured/unique reflections	144244/14895
Number of unique reflections with $I > 2\sigma(I)$	12378
R_{int}	0.0556
GOOF	1.076
R_1, wR_2 ($I > 2\sigma(I)$)	0.0368, 0.0817
R_1, wR_2 (for all data)	0.0502, 0.0878
$\Delta\rho_{max}/\Delta\rho_{min}$, e Å^{-3}	2.08/−1.17

The full set of X-ray diffraction parameters was deposited with the Cambridge Crystallographic Data Centre (CCDC no. 2237815; https://www.ccdc.cam.ac.uk/structures).

The antiradical and antioxidant activities of compounds were assessed in reactions with the DPPH radical and 2,2'-azino-bis(3-ethylbenzothiazoline-6-sulfonic acid) ($ABTS^{\bullet+}$) radical cation and in the CUPRAC assay by known procedures [17–19]. The starting concentration of the DPPH radical was 50 μmol L^{-1}. The antiradical efficiency (AE) was defined by the relation $AE = 1/(EC_{50} \times TEC_{50})$, where EC_{50} is the antioxidant concentration needed to decrease the amount of the DPPH radical by 50% relative to the initial value and TEC_{50} is the time needed to attain the EC_{50} concentration. The IC_{50} value in the ABTS assay was calculated as the minimum concentration of the test compounds needed to decrease the $ABTS^{\bullet+}$ content by 50% relative to the initial value. In the CUPRAC and $ABTS^{\bullet+}$ assays, the absorbances were plotted versus the concentration for the test compounds and Trolox. The Trolox equivalent antioxidant capacity (TEAC) was measured by comparing the slopes of the plots obtained for each compound with the plot for Trolox. The DNA oxidative damage in the presence of AAPH and the test compounds (50 μmol L^{-1}) was performed according to the previously described method [20]. The Wistar rat liver homogenates (1 : 10 w/v) were prepared immediately before use in a phosphate-buffered medium (pH 7.4) by means of a homogenizer. The degree of lipid peroxidation (LP) was assessed from accumulation of carbonyl products, which form a colored complex with thiobarbituric acid (TBA), using the previously described procedures [21, 22].

The antibacterial activity was determined with respect to the *S. aureus* ATCC 29213, *S. aureus* ATCC 6538p, and *E. coli* ATCC 25922 bacterial strains received from the American Type Culture Collection (ATCC, Manassas, Virginia, USA). The minimum inhibitory concentration (MIC, μg/mL) was determined by microdilutions in liquid MHB nutrient medium in accordance with recommendations of the Clinical and Laboratory Standards Institute (CLSI) [23]. The test compounds were dissolved in dimethyl sulfoxide (DMSO) to an initial concentration of 2500 μg mL^{-1}, diluted with MHB, and tested in the

concentration range from 312.50 to 0.61 μg mL^{-1}. The final DMSO concentration was below 12.5% and did not affect the microbial growth. The inoculums were brought to a content of approximately 5×10^5 CFU mL^{-1}. The diluted bacterial cultures in MHB were incubated at 37°C for 24 h. The MIC values were determined visually as the lowest concentration of the test compound providing complete growth inhibition. Each assay was performed in triplicate in two independent experiments. DMSO in 12.5% concentration served as a negative control and ciprofloxacin was used as a positive control.

The cytotoxicity of the compounds in vitro was evaluated using the cell cultures of human breast cancer (MCF-7), lung cancer (A549), and colorectal cancer (HCT-116), received from the American Type Culture Collection (ATCC, Manassas, Virginia, USA). The cells were cultured in DMEM nutrient medium containing 10% fetal calf serum, 2 mM L-glutamine, 1% penicillin and 1% streptomycin at 37°C and 5% CO_2. The complexes were dissolved in DMSO to an initial concentration of 10 mM, and series dilutions in the culture medium were produced. The final DMSO concentration was below 0.1% and had no effect on the cell viability.

The cell viability after exposure to the compounds was determined by MTT assay. The cells (5×10^3 in 190 μL of the culture medium) were seeded in 96-well plates for 24 h and treated with compounds **I**–**V** in concentrations of 0.10–50.00 μM for 72 h. After the treatment, 10 μL of MTT (5.00 mg/mL) was added into each well for 1 h. After incubation, the medium was removed, DMSO (200 μL) was added, and the absorbance was measured at $\lambda = 540$ nm. The IC_{50} values were calculated as the concentration needed to reduce the cell viability by 50% compared to the reference cell growth (100%). Each assay was performed in triplicate in two independent experiments. In the MTT assay, DMSO in 0.1% concentration served as the negative control, while doxorubicin hydrochloride was used as the positive control.

RESULTS AD DISCUSSION

In order to evaluate the effect of a metal ion on the biological activity and redox properties, we synthesized new gold(I) complexes based on the previously obtained Schiff bases (L^nSH) by the exchange reaction with [$(Ph_3P)AuCl$] in 1 : 1 ratio in acetonitrile in the presence of triethylamine as a deprotonating agent (Scheme 1). The reaction was carried out under anaerobic conditions to avoid the side ligand oxidation processes. Complexes **I**–**V** were isolated by filtration in air as bright yellow or red-orange crystalline powders in up to 75% yields.

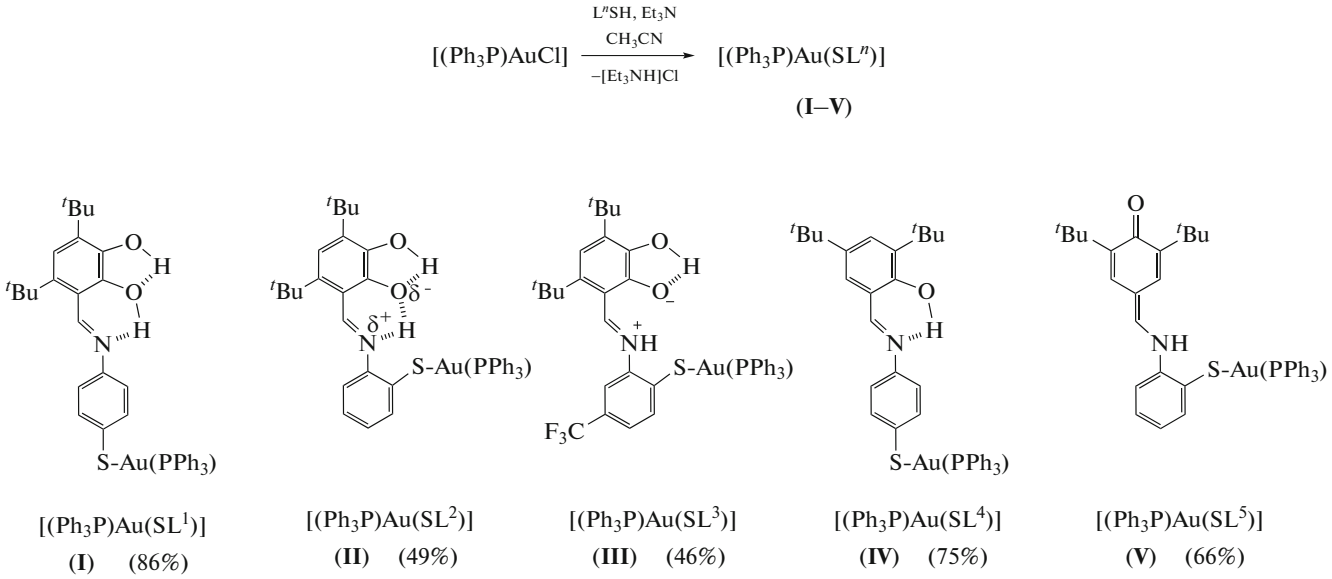

Scheme 1.

The compounds were isolated as finely crystalline powders colored from dark cherry and red (derivatives **I**–**III**) to yellow (compounds **IV** and **V**). The structures of **I**–**V** were established using IR and ^1H and $^{13}C\{^1H\}$ NMR spectroscopy data; the molecular structure of crystalline complex **I** was determined by X-ray diffraction.

Examination of the NMR spectra of the obtained compounds provides data on their molecular structure. The hydroxyl group in position 3 of the catechol

moiety in **I**–**III** is manifested as a singlet at 6.4–6.8 ppm. The second hydroxyl of **I** occurs at 7.4–7.6 ppm (and is superimposed by the multiplet from the phenyl group protons of triphenylphosphine), while in the spectrum of **II**, no signal for the second hydroxyl was detected, which can be attributed to considerable broadening of this signal. Furthermore, unlike **I**, in which the imine proton gives rise to a singlet at 9.30 ppm in the spectrum, in the case of **II**, the CH=N signal gives a doublet at 9.26 ppm, which attests to a considerable intramolecular interaction between the hydroxyl and imine groups and, as a result, to an the intermediate position of the hydrogen atom between nitrogen and oxygen (as shown in Scheme 1 for **II**). The spectrum of **III** exhibits two doublets at 9.32 and 15.90 ppm (with a coupling constant of 2.3 Hz), which can be assigned to the protons of the imine group and iminium cation of the $-CH=N^+H-$ moiety. This means that the proton is completely transferred from the hydroxyl oxygen atom to the nitrogen atom (as shown in Scheme 1 for **III**). This type of prototropic tautomerism was previously noted for the series of catecholaldimines 3-(RN=CH)-4,6-DBCatH_2, where R is an aromatic or aliphatic group, and for their bis-catechol aldimineanalogues [24, 25]. The formation of this type of zwitter-ion structures with the $-CH=N^+H-$ moiety was also found for tin(IV) and antimony(V) complexes with a monodeprotonated form of the catecholaldimine ligand [26].

In the ^{1}H NMR spectrum of **IV**, the singlet for the proton of the only hydroxyl group is shifted downfield to 13.94 ppm. This is indicative of a strong intramolecular OH...N interaction, which is not weakened by the intramolecular OH...O hydrogen bond, as in complex **I**.

In the $^{13}C\{^1H\}$ NMR spectra of **I**–**IV**, the imine group gives peaks in the 158–162 ppm range. Meanwhile, the $^{13}C\{^1H\}$ NMR spectrum of **V** does not exhibit a signal in this range; however, there is a signal at 184.61 ppm falling in the characteristic region of the *o*- and *p*-quinone carbonyl groups. The ^{1}H NMR spectrum of **V** contains a doublet at 9.57 ppm with $^3J(H,H) = 14.4$ Hz, which can be assigned to the CH proton of the =C<u>H</u>–NH– moiety. The spectral features of **V** indicate that this compound does not exist as the phenolic form A, but exists as the *para*-quinone methide form B (Scheme 2). These conclusions are confirmed by IR spectroscopy data. The IR spectrum of **V** shows an intense band at 1622 cm^{-1}, corresponding to the ketone group stretching vibrations, and a narrow intense band at 3284 cm^{-1}, typical of N–H mode of the amino group.

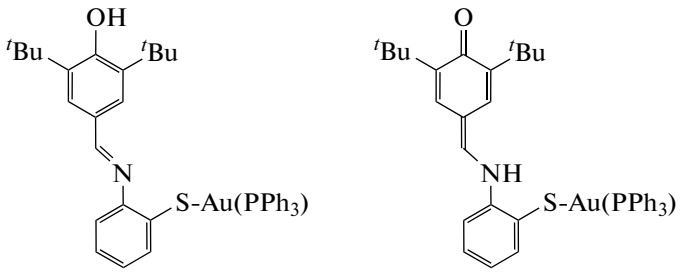

A B

Scheme 2.

The molecular structure of catechol-containing gold complex **I** in the crystalline state was established by X-ray diffraction (Fig. 1). The geometric parameters of the C(1–6) six-membered ring ($d_{average}$(C–C) = 1.406 ± 0.027 Å) and the oxygen–carbon bond lengths (O(1)–C(1), 1.369(3); O(2)–C(2), 1.328(4) Å) are in line with those of previously studied catechols [24, 27, 28]. The Au(1) coordination number is 2, the S(1)Au(1)P(1) bond angle is close to the straight angle (177.1(1)°), and the C(11)S(1)Au(1) bond angle is 98.75(5)°. These bond angles are, in general, quite common for two-coordinate gold(I) compounds of the [(R_3P)Au–S–Ar] type. Indeed, these angles are 178.90° and 105.07° in [(Me_2PhP)Au–S–*p*-C_6H_4COOH] [29]; 174.48° and 108.05° in [(Ph_3P)Au–S–$C_6H_1F_4$] [30]; 174.43° and 108.33° in [(Ph_3P)Au–S–C_6F_5] [31]; 176.6°–178.9° and 102.5°–103.1° in the series of [(Cyclohex$_3$P)Au–S–*o*-C_6H_4-C(O)NH_2], [(Ph_3P)Au–S–*o*-C_6H_4-C(O)NH_2], and [(Et_3P)Au–S–*o*-C_6H_4–C(O)NH_2] [32]; and 176.53° and 104.10° in [(Ph_3P)Au–S–*p*-C_6H_4-NMe_2] [33]. The Au(1)–S(1) and Au(1)–P(1) bond lengths (2.2931(8) and 2.2632(8) Å, respectively) are usual for triaryl/trialkylgold(I) thiolates (2.28–2.31 and 2.25–2.27 Å [33–35]).

The N(1)–C(7) bond is a double bond conjugated with the π-system of the C(1–6) ring. In molecule **I**, there are intramolecular hydrogen bonds (O(1)–H(1)...O(2), 2.133(3); and O(2)–H(2)...N(1), 1.755(3) Å). As a result of these contacts, H(2) is incorporated in the O(2)C(2)C(3)C(7)N(1)H(1) six-

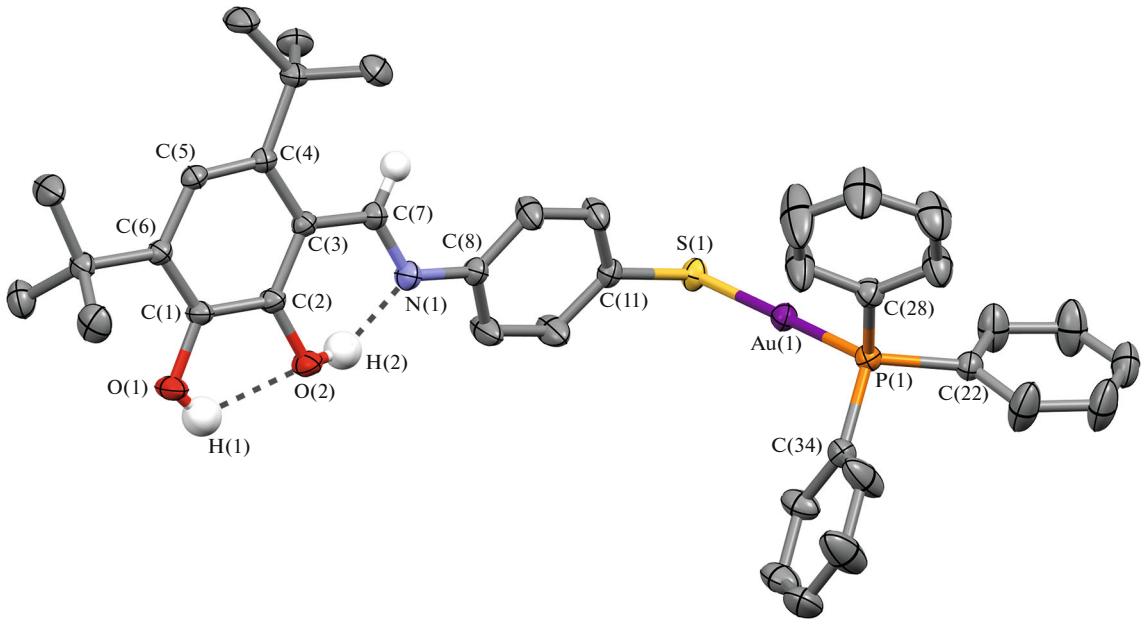

Fig. 1. Structure of molecule **I** in the crystal according to X-ray diffraction data. Ellipsoids are drawn at 30% probability level; hydrogen atoms except for H(1)–H(3) are omitted. Selected bond lengths: Au(1)–P(1), 2.2632(8); Au(1)–S(1), 2.2931(8); P(1)–C(22), 1.809(3); P(1)–C(28), 1.805(3); P(1)–C(34), 1.815(3); S(1)–C(11), 1.787(3); O(1)–C(1), 1.369(3); O(2)–C(2), 1.328(4); N(1)–C(7), 1.295(4); N(1)–C(8) 1.413(3), C(1)–C(2) 1.406(3), C(1)–C(6) 1.382(4), C(2)–C(3) 1.421(3), C(3)–C(4) 1.435(4), C(4)–C(5), 1.379(3); C(5)–C(6), 1.413(3); C(3)–C(7), 1.437(3) Å.

membered ring (the O(2)–C(2)–C(7)–N(1) torsion angle is 2.6(1)°).

Currently, molecular electrochemistry methods are widely used to predict the metabolic pathways of redox-active molecules and to establish the main routes of their chemical transformations in biosystems. The key advantages of the electrochemical approach include the generation of active metabolites under mild conditions; studies in a non-cellular medium; gaining information on the mechanisms of transformations and metabolic pathways of the target compounds from the data of CV, electrolysis, and spectroelectrochemistry; the possibility of preparation of the oxidized metabolites of redox-active compounds and evaluation of their toxicity; and modeling of the reactions of intermediates with biomolecules (glutathione, ascorbic acid, NADH) [36, 37]. Since the molecules of the obtained complexes contain redox-active catechol and phenol moieties, their electrochemical properties were studied by CV in dichloromethane on a GC electrode (Table 2).

The electrochemical oxidation of **I**–**V** has common features: the CV curves show two or three successive anodic processes (Fig. 2).

Table 2. Redox potentials of complexes **I**–**V** determined by CV*

Compound	E_p^{ox1}, V	E_p^{ox2}, V	E_p^{ox3}, V	$E_{1/2}^{red1}$, V	I_a/I_c
[$(Ph_3P)Au(SL^1)$] (**I**)	0.89	1.13	1.60	–1.58	0.95
[$(Ph_3P)Au(SL^2)$] (**II**)	0.89	1.17	1.65	–1.56	0.80
[$(Ph_3P)Au(SL^3)$] (**III**)	0.94	1.19	1.63	–1.46	0.90
[$(Ph_3P)Au(SL^4)$] (**IV**)	0.96	1.25	1.62	–1.87	
[$(Ph_3P)Au(SL^5)$] (**V**)	0.84	1.47		–1.60	
Auranofin [38]	1.10	1.60			
[$(Ph_3P)Au$(4-S-Tol)]** [39]	0.82	1.50			

* CH_2Cl_2, GC electrode, 0.1 M n-Bu_4NClO_4, $c = 2 \times 10^{-3}$ mol/L, Ar, vs. Ag/AgCl/KCl (sat.).
** [$(Ph_3P)Au$(4-S-Tol)] is Au(I) triphenylphosphine p-thiocresolate complex.

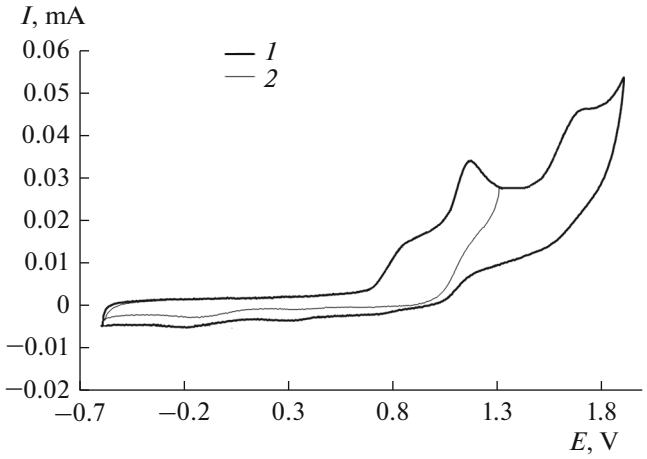

Fig. 2. The oxidation cyclic voltammograms of **II**: (*1*) in the potential range from –0.6 to 1.9 V; (*2*) in the potential range from –0.6 to 1.3 V (CH_2Cl_2, GC anode, Ag/AgCl/KCl, 0.1 M n-Bu_4NClO_4, $c = 2 \times 10^{-3}$ mol/L, argon).

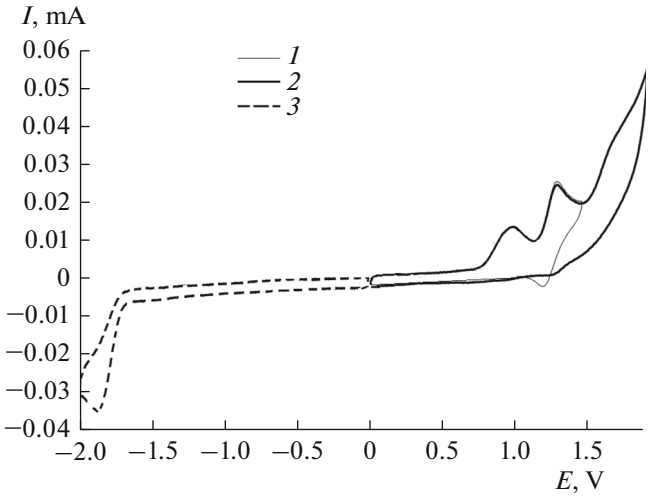

Fig. 3. The cyclic voltammograms of **IV**: (*1*) in the potential range from 0 to 1.45 V; (*2*) in the potential range from 0 to 1.90 V; (*3*) in the potential range from 0 to –2.00 V (CH_2Cl_2, GC electrode, Ag/AgCl/KCl, 0.1 M n-Bu_4NClO_4, $c = 2 \times 10^{-3}$ mol/L, argon).

The first oxidation peak is irreversible for all of the compounds, which attests to a fast chemical step following the electron transfer. This behavior is typical phosphine thiolate gold(I) complexes and is associated with the oxidation of the coordinated thiolate anion to give the thiyl radical and the $[(Ph_3P)Au]^+$ cation [39–42]. This mechanism provides the main route of the electrochemical transformations of gold(I) thiolate derivatives [41, 42]. In the case of the research compounds, the presence of catechol or phenol redox-active groups determines their participation in the second oxidation stage (Fig. 3).

The oxidation potentials (1.13–1.19 V) and the partial reversibility of the observed peaks (I_c/I_a = 0.4–0.5) for the first three compounds imply the involvement of the catechol moiety. The redox transformations of complex **IV** are shown in Scheme 3. The second quasi-reversible peak for **IV** is identical to that observed for the free ligand, which is related to the possibility of electron density delocalization involving the phenol fragment.

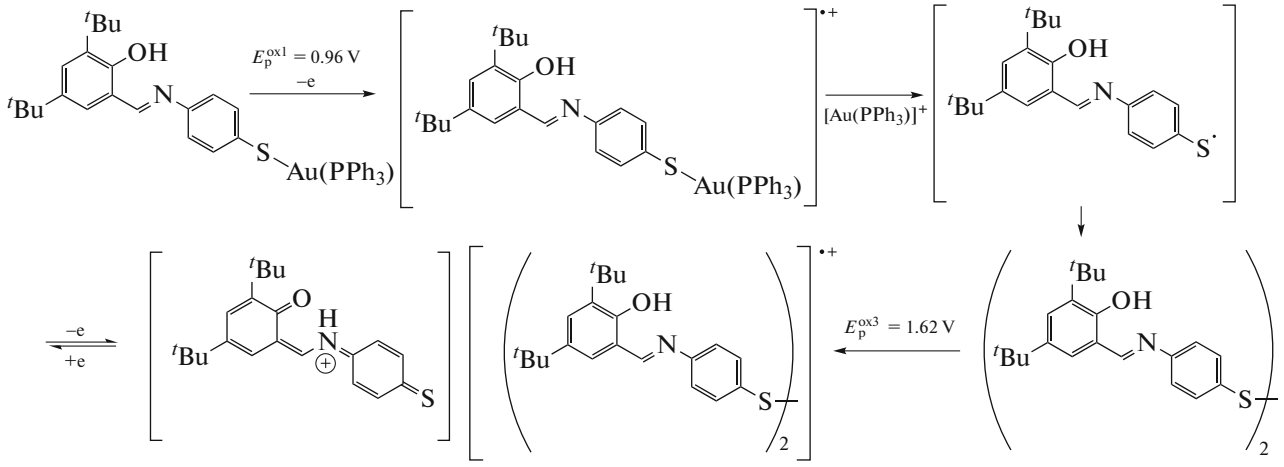

Scheme 3.

The thiyl radicals generated upon the oxidation of **I**–**IV** rapidly dimerize via a parallel reaction, which results in the formation of disulfides, the oxidation peaks of which occur in a narrow range of the CV curve, 1.60–1.65 V, typical of the oxidation of disulfides [42]. In addition, electrooxidation of LS$^\bullet$ may afford a sulfur-cen-

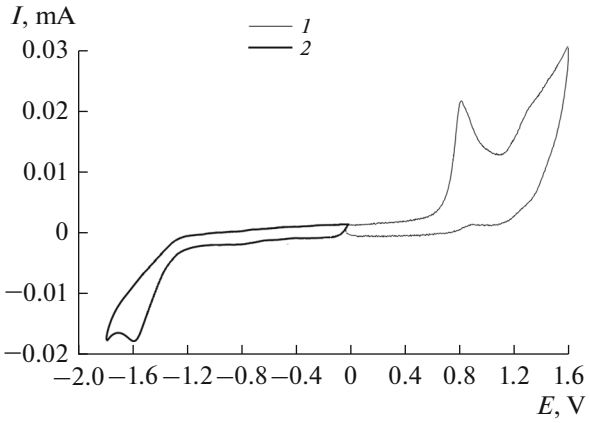

Fig. 4. The cyclic voltammograms of **V**: (*1*) in the potential range from 0 to 1.60 V; (*2*) in the potential range from 0 to –1.80 V (CH_2Cl_2, GC electrode, Ag/AgCl/KCl, 0.1 M n-Bu_4NClO_4, $c = 1.5 \times 10^{-3}$ mol/L, argon).

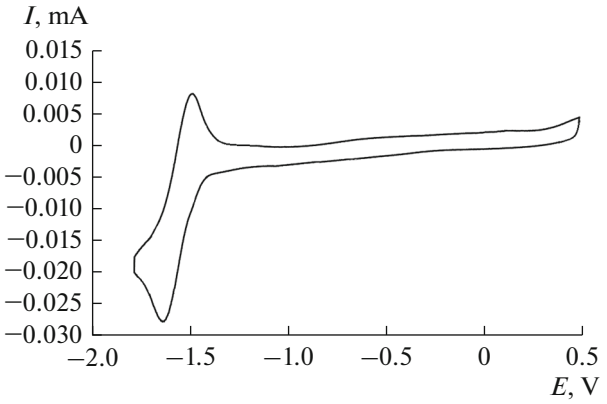

Fig. 5. The reduction cyclic voltammogram of **I** in the potential range from 0.5 to –1.80 V (CH_2Cl_2, GC electrode, Ag/AgCl/KCl, 0.1 M n-Bu_4NClO_4, $c = 2 \times 10^{-3}$ mol/L, argon).

tered cation. The electrophilic attack by this cation on the initial [(Ph_3P)Au(SL)] complex can also yield disulfides. The general chart of the oxidative transformations of the complexes can be represented as follows (Scheme 4).

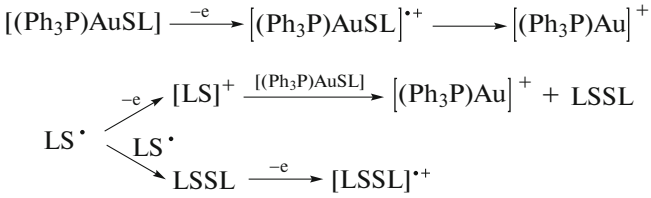

Scheme 4.

Compound **V** with the quinone methide group does not show a clear-cut third oxidation peak, corresponding to the disulfide formation (Fig. 4), and the potential E_p^{ox2} is shifted to the anodic region. In the oxidative activation of **V** and elimination of $[(Ph_3P)Au]^+$, the ligand further undergoes more extensive transformations, resulting in the intramolecular cyclization with hydrogen atom transfer and the possibility of formation of a benzoxazole ring [43].

Analysis of the obtained values of E_p^{ox1} for **I** and **II** demonstrated that the position of the gold-containing moiety relative to the azomethine group has no effect on the oxidation potential. The introduction of the trifluoromethyl substituent into the aromatic ring induces the shift of the E_p^{ox1} to the anodic region by 0.05 V. The replacement of the catechol by the phenol moiety in complexes **I** and **IV** has a similar effect, shifting the oxidation to anodic area. Meanwhile, the presence of the peripheral quinone methide group in **V** does not induce a significant change in the oxidation potential, which is close to that of the Au(I) p-thiocresolate triphenylphosphine complex in dichloromethane [39]. Note that despite the presence of electron-withdrawing imino group in compounds **I**–**V**, their E_p^{ox1} values are located in a more cathodic region than those for auranofin (1.10 V).

The cathodic region for **I**–**III** contains a quasi-reversible one-electron peak corresponding to the formation of relatively stable radical anion species ($I_a/I_c = 0.80$–0.95) (Fig. 5). This behavior is attributable to the participation of the azomethine linker in the redox process [44]. In the case of compound **IV**, this step is irreversible and is shifted to the cathodic region compared to that of **I**.

Compound **V** containing a quinone methide group is also reduced irreversibly, like the complex with a phenol moiety; however, the reduction of **V** occurs at a more anodic potential, which may be indicative of the presence of weak acceptor properties.

Study of the spectral properties of gold(I) complexes in the visible region of the absorption spectrum showed an absorption maximum for **I**–**V** in the 370–390 nm range (**I**, 390 nm ($\varepsilon = 1.48 \times 10^4$ M^{-1} cm^{-1}); **II**, 387 nm ($\varepsilon = 1.16 \times 10^4$ M^{-1} cm^{-1}); **III**, 390 nm

($\varepsilon = 1.01 \times 10^4$ M^{-1} cm^{-1}); **IV**, 384 nm ($\varepsilon = 2.04 \times 10^4$ M^{-1} cm^{-1})). This peak is caused by electron density transfer between the thiolate anion and the azomethine group. A specific feature of **V** is the presence of an intense absorption maximum at $\lambda = 442$ nm ($\varepsilon = 2.84 \times 10^4$ M^{-1} cm^{-1}) shifted to longer wavelengths compared with those of other compounds. An explanation to the higher cytotoxicity of compounds with a quinone methide groups is the ability to bind to the thiol groups of protein molecules and to inhibit the thioredoxin reductase enzyme. To confirm the electron-withdrawing nature of the quinone methide group, model experiments with cyclopentanethiol were carried out. It turned out that none of the compounds, except **V**, reacts with thiols. When 2 equiv. of thiol were added into a solution of complex **V**, the intensity of the absorption maximum at 442 nm rapidly decreased, which was accompanied by discoloration of the solution (Fig. 6).

In the CV curves, a decrease in the current intensity of the cathodic peak corresponding to the reduction of the quinone methide moiety also took place. This behavior of complex **V**, like the behavior of the ferrocene quinone methides studied previously [45], can be attributed to the formation of Michael addition products. The reaction of **V** with cyclopentanethiol is depicted in Scheme 5.

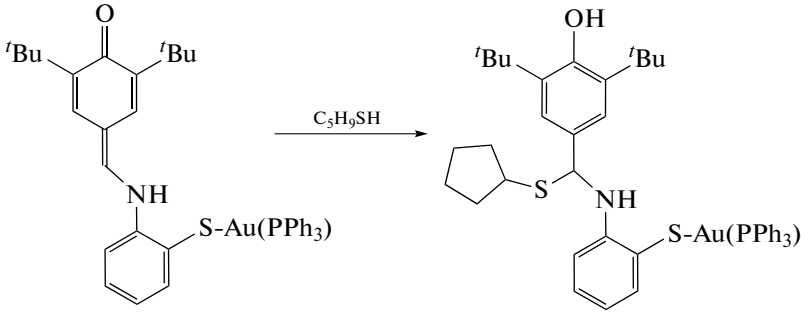

Scheme 5.

The presence of the quinone methide moiety in compound **V**, as well as the presence of gold(I) ion, which inhibits thioredoxin reductase, suggests the possibility of a higher cytotoxicity against cancer cells and a good cytostatic potential, providing inhibition of the target enzyme by different mechanisms. Further studies would make it possible to evaluate the effect of redox-active moieties in the ligand and the metal ion on the biological activity of this type of compounds.

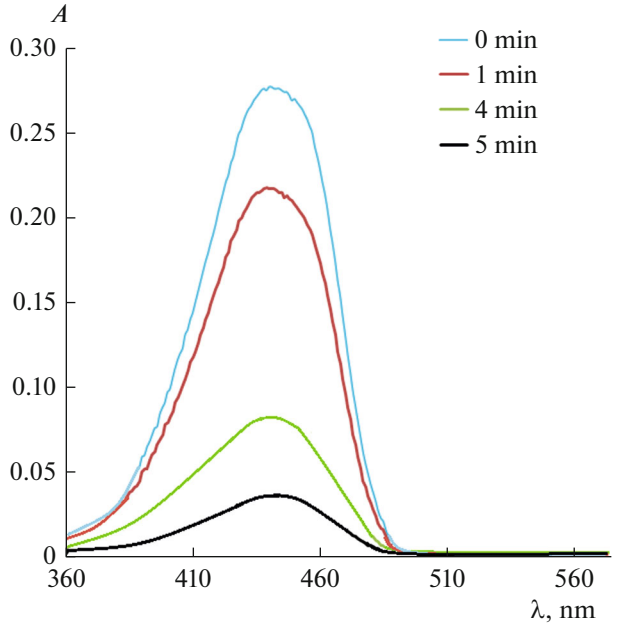

Fig. 6. Absorption spectrum of **V** (0 min) in the presence of 2 equiv. of cyclopentane-1-thiol (1–5 min) (CH_2Cl_2, 298 K, $c = 1 \times 10^{-5}$ mol/L).

A recent progress in the synthesis of new biologically active organometallic and coordination compounds has been related to the preparation of compounds containing, apart from metal atoms, various redox-active groups, privileged heterocyclic scaffolds, and pharmacophore functional groups. Along the way towards the development of pharmacologically active agents, a significant stage is the integrated primary screening using various model reactions and in vitro processes and biochemical systems mimicking physiological conditions. The modern approach to the study of biologically active compounds requires both an integrated evaluation and determination of the contribution of each moiety to the potential activity of the molecule.

We carried out an integrated evaluation of the antiradical activity of compounds **I**–**V** at the molecular level using synthetic radicals, that is, by DPPH assay, using the $ABTS^{\bullet+}$ radical cation, and by the CUPRAC assay based on the determination of the antioxidant activity of a compound in the reduction of copper(II) complex with 2,9-dimethyl-1,10-phenathroline (neocuproine) (Table 3).

The characteristics of complexes **II** and **III** in the DPPH assay were comparable to those of free Schiff

Table 3. EC_{50}, TEC_{50}, and AE (antiradical efficiency) for complexes **I**–**V** and ligands found in DPPH radical assay (CH_2Cl_2, 298 K); IC_{50} and TEAC values found in the $ABTS^{\bullet+}$ assay; reducing activity in the reaction with Cu^{2+} (CUPRAC) expressed in Trolox equivalents (TEAC)

Compound	DPPH			$ABTS^{\bullet+}$		CUPRAC
	EC_{50}, μmol	TEC_{50}, min	AE × 10^3	IC_{50}, μmol	TEAC	TEAC
$[(Ph_3P)Au(SL^1)]$	20.8 ± 0.8	45.0	1.06 ± 0.1	11.0 ± 0.7	1.60 ± 0.14	0.58 ± 0.10
$[(Ph_3P)Au(SL^2)]$	16.4 ± 1.2	13.0	4.30 ± 0.3	15.5 ± 0.9	1.41 ± 0.11	1.46 ± 0.15
$[(Ph_3P)Au(SL^3)]$	14.9 ± 1.2	35.0	1.9 ± 0.3	14.6 ± 0.4	1.52 ± 0.20	0.99 ± 0.11
$[(Ph_3P)Au(SL^4)]$	>100	>120		45.8 ± 1.5	0.37 ± 0.08	0.38 ± 0.05
$[(Ph_3P)Au(SL^5)]$	>100	>120		22.0 ± 0.5	0.54 ± 0.10	0.36 ± 0.04
L^1SH*	10.0 ± 0.5	45.0	2.2 ± 0.4	8.8 ± 0.6	1.88 ± 0.10	1.60 ± 0.09
L^2SH*	16.0 ± 1.1	10 ± 1.5	6.25 ± 0.8	12.1 ± 1.2	1.73 ± 0.23	2.25 ± 0.11
L^3SH*	14.5 ± 0.4	45 ± 0.9	1.5 ± 0.1	12.5 ± 1.0	1.68 ± 0.17	2.03 ± 0.05
L^4SH*	30.0 ± 1.3	5 ± 0.4	6.7 ± 0.8	17.7 ± 1.2	1.07 ± 0.09	0.71 ± 0.07
L^5SH*	10.9 ± 1.1	3 ± 0.5	30.5 ± 3.1	14.0 ± 0.9	1.51 ± 0.09	2.39 ± 0.10
$CatH_2$*	13.1 ± 1.3	60 ± 2.0	1.3 ± 0.2	1.5 ± 0.5	1.27 ± 0.15	0.72 ± 0.05
$[(Ph_3P)AuSR]$**	31.0 ± 2.0					1.05 ± 0.07
Trolox	12.0 ± 0.5	10.3	5.1 ± 0.5	16.0 ± 1.0	1.00 ± 0.03	1.00 ± 0.08

* The data were reported in [12]; ** the data were reported in [7].

bases. The possibility of interaction with a stable radical for these compounds is due to the hydrogen atom abstraction from the catechol group; this is confirmed by EC_{50} values similar to those for 3,5-di-*tert*-butylcatechol. In the case of **I**, EC_{50} increased twofold, with the time needed to reach the equilibrium state (TEC_{50}) being the same; this implies a decrease in the antiradical action compared to that of L^1SH.

As distinct from the initial ligands, binding of the SH group to the gold(I) ion in **IV** and **V** leads to a considerable decrease in their reactivity towards diphenylpicrylhydrazyl. The hydrogen aton abstraction in the reaction with the radical is complicated in the case of **IV**, which is attributable to the formation of an intramolecular hydrogen bond between the phenol OH group and the imine nitrogen atom. In complex **V**, the presence of the electron-withdrawing quinone methide moiety also hampers hydrogen atom abstraction by the radical. Meanwhile, **I**–**III** showed greater antiradical activity than the gold(I) triphosphine thiolate complex with 3,5-di-*tert*-butyl-4-hydroxythiophenolate ligand [34]. The presence of the azomethine linker between the aromatic ring and the phenol group in **IV** leads to a significant decrease in the radical scavenging activity in the DPPH assay.

The IC_{50} values found for the reactions of **I**–**III** with ABTS radical cation, which is a stronger acceptor, were in good agreement with the EC_{50} values found in the DPPH assay. The antioxidant activity (TEAC) of the complexes was 1.4–1.6 times higher than the value for the Trolox, a water-soluble analogue of vitamin E. Analysis of the characteristics obtained for the complexes demonstrated a slight decrease in the antioxidant properties compared to those of free ligands. Complexes **IV** and **V** act as weak electron donors towards $ABTS^{\bullet+}$. The TEAC values were similar to those found in the CUPRAC assay; this generally attests to relatively low antioxidant capacity of these compounds. In the initial Schiff bases, the presence of the free SH group makes the major contribution to the antioxidant activity. The reactions of **I**–**III** with the neocuproine copper(II) complex show a moderate activity, and only for complex **II**, the results are superior to the data for Trolox.

The inhibiton of the radical chain processes via scavenging of the reactive radicals is the key feature of most known antioxidants. The presence of phenol and catechol groups in the ligands accounts for the abovementioned neutralizing activity of gold(I) complexes towards synthetic radicals. In the next stage, it was interest to evaluate the effect of the target compounds on the DNA and lipid damage promoted by the ROO radicals. The intense generation of the reactive oxygen species (ROS), inhibition of antioxidant defense enzymes, and the promotion of oxidative stress can lead to damage to biomacromolecules such as proteins, lipids, and DNA. Gold(I) compounds do not react with DNA. However, it was noted previously that in the presence of gold(I) complexes, thioredoxin reductase is inhibited, and this is accompanied by an

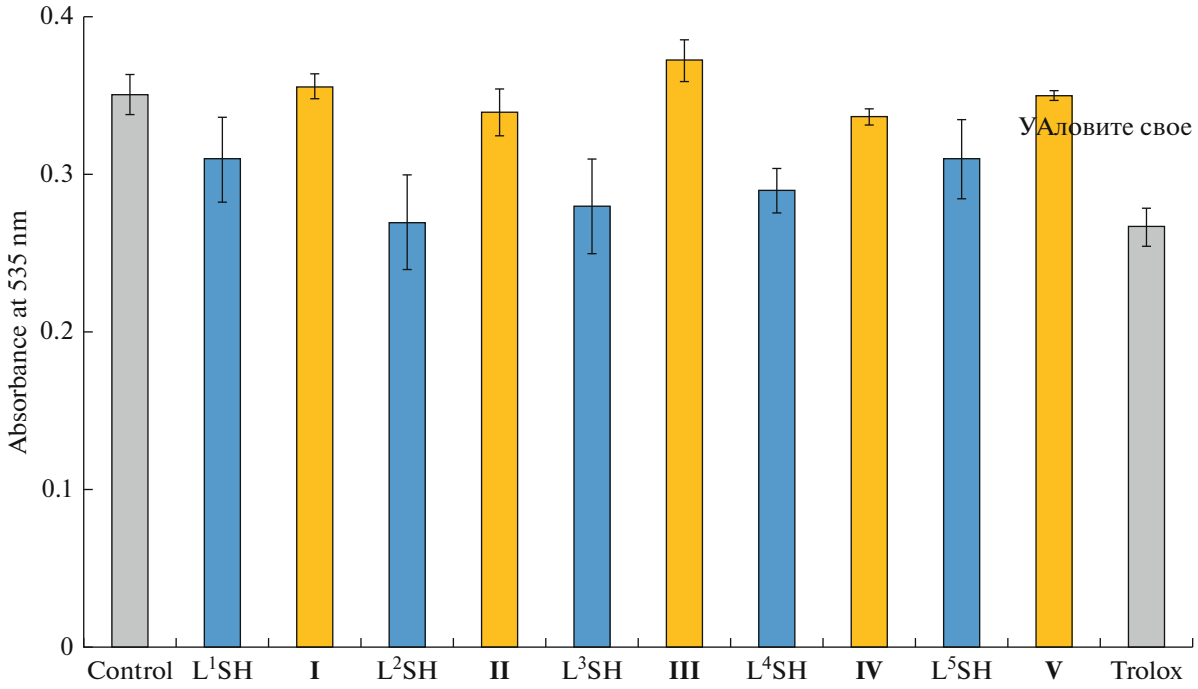

Fig. 7. The variety of the TBARS absorbance upon the oxidative damage of DNA (2.0 mg mL^{-1}) induced by AAPH promoter (40 mmol L^{-1}) in the presence of **I**–**V** (50 μmol), ligands (L^1SH–L^5SH), and Trolox (control without addition of test compounds).

increase in ROS level, which can lead to damage to deoxyribose and disrupt the DNA integrity [46].

The antioxidant activity of **I**–**V** was studied in the promoted oxidative damage of DNA with 2,2'-azobis(2-amidinopropane) dihydrochloride (AAPH) [12], which decomposes at 37°C to give peroxyl radicals, initiating the damage of DNA deoxyribose moieties. The carbonyl compounds formed in the reaction react with thiobarbituric acid, thus forming colored products (TBARS) (λ_{max} = 535 nm). Comparative data on the reactivity of gold complexes **I**–**V** and previously obtained results for the ligands are summarized in Fig. 7.

Unlike the initial Schiff bases, **I**, **II**, **IV**, and **V** have almost no clear-cut effect on the oxidative damage of DNA molecules: the absorbances are comparable with that in the control experiment within the measurement error. A weak promoting action (6.5%) is observed only for compound **III**. The results confirm the absence of a pronounced effect of the complexes on DNA molecules in this assay.

The inhibition of some antioxidant defense enzymes and reactions with the thiol groups of proteins under the action of gold complexes can lead to ROS generation, damage of lipids, or disruption of lipid metabolism [47, 48]. In addition, previously, we showed that the initial Schiff bases L^1SH–L^3SH containing catechol moieties markedly intensify the LP process in vitro. Meanwhile, sulfur-containing Schiff bases with the phenol group may inhibit LP [43]. Hence, we studied the effect of **I**–**V** and L^4SH on the non-enzymatic Fe^{2+}-promoted peroxidation of lipids of the Wistar rat liver homogenate in vitro. The remote effects of gold(I) complexes on LP were evaluated by measuring the concentration of TBARS after 3, 24, and 48 h. The samples of the rat liver homogenates were divided as follows: control containing no additives, five samples containing substances **I**–**V** (100 μmol) and L^4SH. The TBARS concentration was determined from the change in the absorbance of solutions at 535 nm (Fig. 8).

Analysis of the results demonstrated that after 3 h of incubation, all of the complexes have a moderate inhibitory effect, decreasing the TBARS level by 13–37%, as distinct from the free Schiff bases studied previously. The highest antioxidant activity was found for compound **IV**. An increase in the incubation time leads to LP intensification in the control sample. The antioxidant to pro-oxidant inversion was detected for **III** after 24 h. The addition of complex **III** leads to an increase in the content of lipid oxidation products over time, indicating its promoting action. The decrease in the TBARS concentration by 12–23% for **I** and **II** confirms their moderate antioxidant activities. For compound **IV**, containing a sterically hindered phenol group, the inhibitory effect increases over time, as the TBARS content regularly decreases by 37 (3 h) and 48% (24 h) compared to the control sample. Meanwhile, the free ligand also efficiently inhibits LP. Gold complex **V** with a quinone methide moiety has no sig-

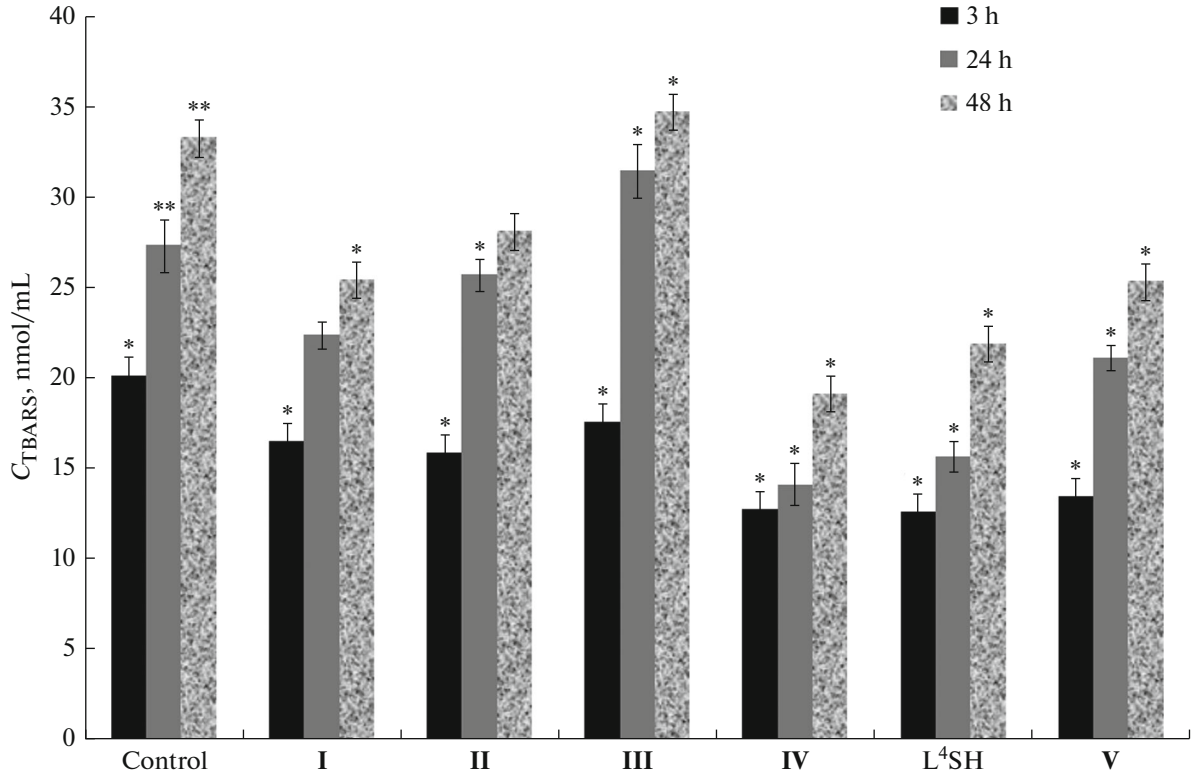

Fig. 8. The level of TBARS in rat liver homogenates in vitro in the presence of compounds **I**–**V** and Schiff bases L^4SH during incubation (3, 24, 48 h) (concentration of test compounds: 100 μmol; control without the test compounds; the average values with standard deviations are given (* $p < 0.001$; ** $p < 0.005$)).

nificant promotion effect; conversely, it has a moderate inhibitory action. This may be due to the possibility of quinone methide trapping by a group of peroxyl radicals, which was observed previously for *o*-benzoquinones [49]. Unlike the previously studied gold(I) thiolate complexes with heterocyclic thiols, which actively promote cell membrane peroxidation [47], the presence of an antioxidant group induces an opposite effect [5]. In our case, the gold coordination to the thiol group as well as the presence of redox-active catechol or phenol groups in compounds **I**, **II**, and **IV** are favorable for the antioxidant activity. Conversely, the introduction of the trifluoromethyl substituent into the iminothiophenolate moiety induces inversion of antioxidant to prooxidant properties with increasing incubation time.

Auranofin and gold(I) phosphine complexes with various thiolate ligands possess not only cytotoxicity against cancer cells, but also pronounced antibacterial activity against gram-positive bacteria, in particular *Staphylococcus aureus* [50–52]. The sulfur-containing Schiff bases L^1SH–L^3SH with a catechol group synthesized previously exhibited a moderate bacteriostatic action against *Staphyococcus aureus* [12]. Therefore, a similar effect was expected for **I**–**V**. The antibacterial activity of the complexes was studied against *Staphylococcus aureus* and *Escherichia coli* bacterial strains (Table 4).

As indicated by the obtained MIC values, the coordination of the thiol group to the gold(I) atom results in a considerable decrease in the bacteriostatic action of complexes **II** and **III** in comparison with the starting ligands. In the case of **I** and L^1SH, MIC indexes are similar. Gold compounds **I**–**V** proved to be inactive against *Escherichia coli*, like most of the ligands. The Schiff base L^4SH with a sterically hindered phenol moiety did not show antibacterial activity [12], while the MIC values for compound $[(Ph_3P)Au(SL^4)]$ were comparable with those for complexes **I** and **II** against *Staphylococcus aureus* ATCC 29213. Compound **V** with the quinone methide group shows a moderate antibacterial activity, unlike the starting iminothiol. This behavior can be attributed to the presence of a quinone methide group capable of binding to the cysteine residues of protein molecules and inhibiting thioredoxin reductase; this results in the disruption of the redox balance in the cells and gives rise to an antibacterial effect [53].

A key target for the considered gold(I) complexes, apart from thioredoxin reductase, is the NAD(P)H quinone oxidoreductase 1 (NQO1), involved in two-electron reduction of quinones to hydroquinones and catechols [54]. The oxidation of catechol groups in

Table 4. Antibacterial activity of **I**–**V** and Schiff bases against bacterial strains in vitro

Compound	Minimum inhibitory concentration (MIC), μg/mL		
	Staphylococcus aureus ATCC 29213	*S. aureus* ATCC 6538p	*Escherichia coli* ATCC 25922
$[(Ph_3P)Au(SL^1)]$	39.06	78.13	
$[(Ph_3P)Au(SL^2)]$	39.06	78.13	
$[(Ph_3P)Au(SL^3)]$	19.53	19.53	
$[(Ph_3P)Au(SL^4)]$	39.06		
$[(Ph_3P)Au(SL^5)]$	9.77	9.77	
L^1SH*	39.06	19.53	
L^2SH*	1.22	1.22	39.06
L^3SH*	2.44	4.88	
Ciprofloxacin	0.125	0.125	0.008

* The data were reported in [12].

Table 5. Cytotoxicity values IC_{50} (μmol) for complexes **I**–**V** and Schiff bases against various cancer cell lines

Compound	IC_{50}, μmol		
	A-549	MCF-7	HCT-116
$[(Ph_3P)Au(SL^1)]$	36.03 ± 1.04	8.97 ± 0.22	5.47 ± 0.30
$[(Ph_3P)Au(SL^2)]$	10.31 ± 0.92	11.95 ± 0.76	8.02 ± 0.43
$[(Ph_3P)Au(SL^3)]$	2.47 ± 0.10	10.46 ± 0.65	15.73 ± 0.89
$[(Ph_3P)Au(SL^4)]$	32.78 ± 0.97	17.57 ± 1.17	9.11 ± 0.33
$[(Ph_3P)Au(SL^5)]$	7.43 ± 0.44	4.31 ± 0.27	2.83 ± 0.16
L^1SH*	3.53 ± 0.31	7.43 ± 0.70	11.03 ± 0.17
L^2SH*	2.55 ± 0.02	3.32 ± 0.01	4.26 ± 0.01
L^3SH*	2.99 ± 0.02	4.71 ± 0.41	6.13 ± 0.09
L^4SH*	30.63 ± 1.35	43.19 ± 4.27	25.50 ± 0.99
Cisplatin**	9.02 ± 0.90	15.2 ± 1.10	11.20 ± 1.90
Auranofin***	6.49 ± 0.71	6.21 ± 0.89	

* The data were reported in [12]; ** the data were reported in [58], *** the data were reported in [59].

compounds **I**–**III** by various enzymatic systems, including P450s, cyclooxygenase (COX-2), peroxidases, tyrosinase, and xanthine oxidase, would lead to the generation of reactive oxygen species and *o*-benzoquinones. Enzyme NQO1 in healthy tissues favors the reduction of quinoid compounds and neutralization of ROS; at the same time, this enzyme also has a protective effect in cancer cells by deactivating enhanced amounts of ROS [55]. An increase in the NQO1 expression level is observed in many types of cancer cells including lung, breast, pancreatic, and colon cancers, whereas the level of this enzyme in healthy tissues is relatively low [56]. Therefore, we studied the cytotoxicity of these compounds against MCF-7 (human breast cancer), A-549 (adenocarcinoma human alveolar basal epithelial), HCT-116 (human colon cancer) cells characterized by increased NQO1 level using the modern and popular MTT assay [57] (Table 5).

Analysis of the results demonstrates that the IC_{50} values for gold(I) complexes with a catechol moiety generally increase compared to those of the initial Schiff bases. The IC_{50} values for free ligands L^1SH–L^3SH are less than 10 μmol, i.e., they are more active than cisplatin, but show no clear-cut selectivity to a particular cell line. For **I**–**III**, the decrease in the cytotoxicity predominates; however, unlike the ligands,

they show selectivity to particular cell lines. The IC_{50} value of complex **I** for the HTC-116 colon cancer cells decreases twofold compared to the results obtained previously in the presence of L^1SH, with the activity being higher than that of cisplatin (Table 5). Complex **III** has a more pronounced effect on IC_{50} determined on A-549 lung cancer cells than on other cell lines, which implies a selectivity of action. This compound appears to be more active than auranofin or cisplatin. The coordination of the thiol group in the phenol-containing Schiff bases to the gold(I) ion in complex **IV** leads to lower IC_{50} values for MCF-7 and HTC-116 cells, unlike the coordination in **I**–**III**. An opposite effect was found for the previously studied gold(I) triphenylphosphine complex with 3,5-di-*tert*-butyl-4-hydroxythiophenolate ligand possessing antioxidant activity: the cytotoxicity (IC_{50} > 50 μmol) against MCF-7 and HTC-116 cells significantly decreased compared to that of the initial salt [(Ph_3P)AuCl] [6]. Compound **IV** showed a higher selectivity to HTC-116 cells. Unlike compound **IV**, quinone methide-containing compound **V** has markedly higher cytotoxicity against all cell lines. The IC_{50} values for this compound are comparable with results for auranofin. Thus, the position of the azo linker with respect to the gold-containing moiety, the nature of the substituents in the iminothiophenol moiety, and the type of the redox-active group (catechol, phenol, or quinone methide) allow one to vary the selectivity of cytotoxic action against the considered cancer cell lines compared to the initial Schiff bases.

Thus, the reaction of sulfur-containing Schiff bases with [(Ph_3P)AuCl] leads to the formation of a series of gold(I) phosphine thiolate complexes. The molecular structure of complex **I** was studied by X-ray diffraction. The complex has intramolecular hydrogen bonds between the catechol hydroxyl groups and the imine nitrogen atom. Study of the electrochemical properties of the complexes showed that oxidation of compounds **I**–**V** is irreversible in the first step and leads to Au–S bond cleavage followed by the dimerization of thiyl radicals. The presence of additional redox-active groups causes a second redox transition. Cyclic voltammetry measurements for **I**–**III** showed the formation of relatively stable radical anions in the cathodic region, while in the case of **IV** and **V**, this step is irreversible. Analysis of the antiradical activity of gold(I) complexes against synthetic radicals attests to a general trend of decreasing the neutralizing properties of the complexes in comparison with the ligands. Complexes **I**–**V** have no significant effect on the DNA damage in the presence of radical promoters. Meanwhile, **I**, **II**, **IV**, and **V** have a pronounced antioxidant effect on the lipid peroxidation in the Wistar rat liver homogenate. The antibacterial activity of **I**–**IV** is comparable to or lower than that of Schiff bases. In the case of compound **V**, the presence of the quinone methide group promotes the bacteriostatic effect compared to the initial ligand.

Analysis of the cytotoxicity characteristics of the complexes with respect to the studied cells revealed their greater selectivity to certain types of cancer cells compared to that of Schiff bases. Compound **V** was characterized by the lowest IC_{50} value in the series of the prepared gold(I) complexes, which attests to its high cytotoxicity caused by the presence of the quinone methide moiety. By varying the type of the redox-active group (catechol, phenol, or quinone methide), substituents in the iminothiophenol moiety, or position of the imino group relative to the gold-containing moiety, it is possible to control the selectivity of the cytotoxic action against the considered cancer cell lines compared to the starting Schiff bases.

FUNDING

This study was supported by the Russian Foundation for Basic Research (project no. 19-29-08003) and by State Assignment (no. 123031400121-0).

CONFLICT OF INTEREST

The authors of this work declare that they have no conflicts of interest.

REFERENCES

1. Herrera, R.P. and Gimeno, M.C., *Chem. Rev.*, 2021, vol. 121, no. 14, p. 8311.
2. Galassi, R., Luciani, L., and Wang, J., *Biomolecules*, 2022, vol. 12, p. 80.
3. Van der Westhuizen, D., Bezuidenhout, D.I., and Munro, O.Q., *Dalton Trans.*, 2021, vol. 50, p. 17413.
4. Chupakhin, E. and Krasavin, M., *Expert Opin. Ther. Pat.*, 2021, vol. 31, no. 8, p. 745.
5. Shpakovsky, D.B., Shtil, A.A., Kharitonashvili, E.V., et al., *Metallomics*, 2018, vol. 10, p. 406.
6. Milaeva, E.R., Shpakovsky, D.B., Gracheva, Y.A., et al., *Pure Appl. Chem.*, 2020, vol. 92, no. 8, p. 1201.
7. Antonenko, T.A., Gracheva, Yu.A., Shpakovsky, D.B., et al., *J. Organomet. Chem.*, 2022, vol. 960, p. 122191.
8. Bian, M., Wang, X., Sun, Y., et al., *Eur. J. Med. Chem.*, 2020, vol. 193, p. 112234.
9. Sun, Y., Lu, Y., Bian, M., et al., *Eur. J. Med. Chem.*, 2021, vol. 211, p. 113098.
10. Babgi, B.A., Alsayari, J., Alenezi, H.M., et al., *Pharmaceutics*, 2021, vol. 13, p. 461.
11. Yoshida, T., Onaka, S., and Shiotsuka, M., *Inorg. Chimica Acta*, 2003, vol. 342, p. 319.
12. Smolyaninov, I.V., Burmistrova, D.A., Arsenyev, M.V., et al., *ChemistrySelect*, 2021, vol. 6, no. 39, p. 10609.
13. Gordon, A. and Ford, R., *The Chemist's Companion: A Handbook of Practical Data, Techniques, and References*, New York: Wiley, 1972.

14. *CrysAlisPro, version 1.171.38.41*, Rigaku Oxford Diffraction, 2015.

15. Sheldrick, G.M., *Acta Crystallogr. Sect. A: Found. Adv.*, 2015, vol. 71, p. 3.

16. Sheldrick, G.M., *Acta Crystallogr. Sect. C: Struct. Chem.*, 2015, vol. 71, p. 3.

17. Bondet, V., Brand-Williams, W., and Berset, C., *Food. Sci. Technol.*, 1997, vol. 30, no. 6, p. 609.

18. Re, R., Pellergrini, N., Proteggente, A., et al., *Free Rad. Biol. Med.*, 1999, vol. 26, nos. 9/10, p. 1231.

19. Özyürek, M., Güçlü, K., Tütem, E., et al., *Anal. Methods*, 2011, vol. 3, p. 2439.

20. Smolyaninov, I.V., Pitikova, O.V., Korchagina, E.O., et al., *Bioorg. Chem.*, 2019, vol. 89, p. 103003.

21. Stroev, E.N. and Makarova, V.G. *Praktikum po biologicheskoi khimii* (Laboratory Works in Biological Chemistry), Moscow: Vysshaya shkola, 1986.

22. Smolyaninov, I.V., Burmistrova, D.A., Arsenyev, M.V., et al., *Molecules*, 2022, vol. 27, no. 10, p. 3169.

23. *CLSI, Methods for Dilution Antimicrobial Susceptibility Tests for Bacteria That Grow Aerobically. Approved Standards*, 10th edn. CLSI document M07-A10. Wayne, PA: Clinical and Laboratory Standards Institute, 2015.

24. Astaf'eva, T.V., Arsenyev, M.V., Rumyantcev, R.V., et al., *ACS Omega*, 2020, vol. 5, no. 35, p. 22179.

25. Arsenyev, M.V., Baranov, E.V., Chesnokov, S.A., et al., *Russ. Chem. Bull.*, 2013, vol. 62, no. 11, p. 2394.

26. Baryshnikova, S.V., Bellan, E.V., Poddel'sky, A.I., et al., *Eur. J. Inorg. Chem.*, 2016, vol. 2016, no. 33, p. 5230.

27. Poddel'sky, A.I., Arsenyev, M.V., Astaf'eva, T.V., et al., *J. Organomet. Chem.*, 2017, vol. 835, p. 17.

28. Arsenyev, M.V., Astafeva, T.V., Baranov, E.V., et al., *Mendeleev Commun.*, 2018, vol. 28, p. 76.

29. Helmstedt, U., Lebedkin, S., Hocher, T., et al., *Inorg. Chem.*, 2008, vol. 47, p. 5815.

30. Watase, S., Kitamura, T., Kanehisa, N., et al., *Acta Crystallogr., Sect. C: Cryst. Struct. Commun.*, 2004, vol. 60, p. m104.

31. Watase, S., Kitamura, T., Kanehisa, N., et al., *Chem. Lett.*, 2003, vol. 32, p. 1070.

32. Kang, J.-G., Cho, H.-K., Park, C., et al., *Inorg. Chem.*, 2007, vol. 46, p. 8228.

33. Ahmed, L.S., Clegg, W., Davies, D.A., et al., *Polyhedron*, 1999, vol. 18, p. 593.

34. Milaeva, E.R., Shpakovsky, D.B., Dyadchenko, V.P., et al., *Polyhedron*, 2017, vol. 127, p. 512.

35. Yoshida, T., Onaka, S., and Shiotsuka, M., *Inorg. Chim. Acta*, 2003, vol. 342, p. 319.

36. Jones, A.M., Rahman, M.H., and Bal, M.K., *ChemElectroChem.*, 2020, vol. 6, no. 16, p. 4093.

37. Silva, T.L., Maria de Lourdes, S.G., de Azevedo, Ferreira, F.R., et al., *Curr. Opin. Electrochem.*, 2020, vol. 24, p. 79.

38. Mohamed, A.A., Bruce, A.E., and Bruce, M.R.M., *Metal-Based Drugs*, 1999, vol. 6, nos. 4–5, p. 233.

39. Chen, J., Jiang, T., Wei, G., et al., *J. Am. Chem. Soc.*, 1999, vol. 121, p. 9225.

40. Mohamed, A., Chen, J., Bruce, A.E., et al., *Inorg. Chem.*, 2003, vol. 42, p. 2203.

41. Abdou, H.E., Mohamed, A.A., Fackler, J.P., Jr., et al., *Coord. Chem. Rev.*, 2009, vol. 253, p. 1661.

42. Kupiec, M., Ziółkowski, R., Massai, L., et al., *J. Inorg. Biochem.*, 2019, vol. 198, p. 110714.

43. Smolyaninov, I.V., Poddel'sky, A.I., Baryshnikova, S.V., et al., *Applied Organometal. Chem.*, 2018, vol. 32, p. e4121.

44. Baryshnikova, S.V., Poddel'sky, A.I., Bellan, E.V., et al., *Inorg. Chem.*, 2020, vol. 59, p. 6774.

45. Vessières, A., Wang, Y., McGlinchey, M.J., et al., *Coord. Chem. Rev.*, 2021, vol. 430, p. 213658.

46. Nobili, S., Mini, E., Landini, I., et al., *Med. Chem. Res.*, 2010, vol. 30, p. 550.

47. Abás, E., Pena-Martínez, R., Aguirre-Ramírez, D., et al., *Dalton Trans.*, 2020, vol. 49, p. 1915.

48. Luo, J.M., Ma, X., Jiang, W., et al., *Eur. J. Med. Chem.*, 2022, vol. 232, p. 114168.

49. Smolyaninov, I.V., Kuzmin, V.V., Arsenyev, M.V., et al., *Russ. Chem. Bull.*, 2017, vol. 7, p. 1217.

50. Thangamani, S., Mohammad, H., Abushahba, M.F.N., et al., *Sci. Rep.*, 2016, vol. 6, p. 22571.

51. de Almeida, A.M., de Oliveira, B.A., de Castro, P.P., et al., *Biometals*, 2017, vol. 30, p. 841.

52. Liu, Y., Lu, Y., Xu, Z., et al., *Drug Discov. Today*, 2022, vol. 27, no. 7, p. 1961.

53. Stenger-Smith, J.R. and Mascharak, P.K., *ChemMedChem.*, 2020, vol. 15, no. 18, p. 2136.

54. Bolton, J.L. and Dunlap, T., *Chem. Res. Toxicol.*, 2017, vol. 30, p. 13.

55. Madajewski, B., Boatman, M.A., Chakrabarti, G., et al., *Mol. Cancer Res.*, 2016, vol. 14, p. 14.

56. Parkinson, E.I. and Hergenrother, P.J., *Acc. Chem. Res.*, 2015, vol. 48, no. 10, p. 2715.

57. Zhang, K., Chen, D., Ma, K., et al., *J. Med. Chem.*, 2018, vol. 61, p. 6983.

58. Antonenko, T.A., Shpakovsky, D.B., and Berseneva, D.A., et al., *J. Organomet. Chem.*, 2020, vol. 909, p. 121089.

59. Fereidoonnezhad, M., Mirsadeghi, H.A., Abedanzadeh, S., et al., *New J. Chem.*, 2019, vol. 43, p. 13173.

Translated by Z. Svitanko